Nuclear Engineering and Technology 54 (2022) 2427–2434

Contents lists available at ScienceDirect

Nuclear Engineering and Technology

journal homepage: www.elsevier.com/locate/net

Original Article

Order–disorder structural tailoring and its effects on the chemical stability of $(Gd, Nd)_2(Zr, Ce)_2O_7$ pyrochlore ceramic for nuclear waste forms

Yan Wang [a, b], Jin Wang [a, b, *], Xue Zhang [b], Nan Li [b], Junxia Wang [b, **], Xiaofeng Liang [c]

[a] Fundamental Science on Nuclear Wastes and Environmental Safety Laboratory, Southwest University of Science and Technology, Mianyang, 621010, Sichuan, China
[b] School of Materials Science and Engineering, Southwest University of Science and Technology, Mianyang, Sichuan, 621010, China
[c] Sichuan College of Traditional Chinese Medicine, Mianyang, 621000, Sichuan, China

ARTICLE INFO

Article history:
Received 29 November 2021
Received in revised form
26 January 2022
Accepted 1 February 2022
Available online 2 February 2022

Keywords:
(Gd
$Nd)_2(Zr$
$Ce)_2O_7$ pyrochlore ceramics
Nuclear waste immobilization
Order-disorder structural tailoring
Co-doping
Chemical stability difference

ABSTRACT

Series of unequal quantity Nd/Ce co-doped ceramic nuclear waste forms, $(Gd, Nd)_2(Zr, Ce)_2O_7$, were prepared to tailor its ordered pyrochlore or disordered fluorite structure. The phase transition, micro-topography, and elemental composition of the ceramic samples were systematically investigated, especially the effect of order-disorder structure on the chemical stability. It was confirmed that unequal quantity of Nd/Ce could synchronously replace the Gd/Zr-sites of $Gd_2Zr_2O_7$. And the phase transition of order-disorder structure could be successfully tailored by regulating the average cationic radius ratio of $(Gd, Nd)_2(Zr, Ce)_2O_7$ series. The elements of Gd, Nd, Zr, and Ce are uniformly distributed in the ordered or disordered structures. The MCC-1 leaching results showed that $(Gd, Nd)_2(Zr, Ce)_2O_7$ pyrochlore ceramic nuclear waste forms had excellent chemical stability, whose elements' normalized leaching rates were as low as 10^{-4} -10^{-7} $g \cdot m^{-2} \cdot d^{-1}$ after 7 days. In particular, the chemical stability of disordered structure was superior to that of ordered structure. It was proposed that the force constant and the closest packing were changed with the structure transformation resulting the chemical stability difference.

1. Introduction

With the rapid development of civilian nuclear power and the retirement of nuclear facilities, a tremendous accumulation of high-level radioactive wastes (HLWs) is inevitably generated, which are worthy of attention and resolution [1,2]. Ringwood explored the Synthetic Rock (Synroc) as a futuristic alternate matrix for HLWs immobilization [3]. Kinds of mineral analogue synroc, such as zirconolite [4], pyrochlore [5], perovskite [6], and monazite [7], were extensively researched [8,9]. In recent years, gadolinium zirconate pyrochlore ($Gd_2Zr_2O_7$) has been regarded as a potential material for immobilizing HLWs due to its remarkable thermodynamic stability, excellent chemical stability, good radiation stability and high waste loading capacity [10–13]. The crystal structure of $Gd_2Zr_2O_7$ pyrochlore, classified as $A_2B_2O_7$ type, possesses structural flexibility and composition diversity through A- and B-doping. The specific cations can be incorporated into A/B sites of $A_2B_2O_7$ with similar ionic radius and equivalent valence states [14,15]. Therefore, many radioactive actinides, such as minor actinides (MA) and Pu, can be immobilized into the $Gd_2Zr_2O_7$ crystal lattice [12,16–18]. According to the cationic radius ratio of $A_2B_2O_7$, $r(A^{3+})/r(B^{4+})$, the crystal structures of $A_2B_2O_7$ include the disordered defect-fluorite phase ($r(A^{3+})/r(B^{4+}) < 1.46$), the ordered pyrochlore phase ($1.46 < r(A^{3+})/r(B^{4+}) < 1.78$), and the monoclinic crystalline phase ($r(A^{3+})/r(B^{4+}) > 1.78$) [19,20]. The $r(A^{3+})/r(B^{4+})$ value of 1.4625 for $Gd_2Zr_2O_7$ just stands on the critical line of order-disorder structure. Distinctly, the order-disorder structure of $A_2B_2O_7$ is sensitive to the average $r(A^{3+})/r(B^{4+})$ value, which is closely related to the functional property of pyrochlore. Basing on its performance requirements, the order-disorder structure of $Gd_2Zr_2O_7$-doped matrix can be theoretically tailored by varying doping cation types and contents.

It was reported that Nd and Ce are the two most analogue

* Corresponding author. Fundamental Science on Nuclear Wastes and Environmental Safety Laboratory, Southwest University of Science and Technology, Mianyang, 621010, Sichuan, China.
** Corresponding author.
E-mail addresses: wjin761026@163.com (J. Wang), wjunxia2002@163.com (J. Wang).

https://doi.org/10.1016/j.net.2022.02.001

elements for MA and Pu, respectively [5,21]. The single substitution of A- and B-site and equal quantity co-doping in A/B-sites for $Gd_2Zr_2O_7$ pyrochlore have been extensively researched [18,22–24]. Besides, the A- and B-sites of $A_2B_2O_7$ can also be unequal quantity [25] even aliovalent cation [26] co-substituted simultaneously, which can further neatly take advantage of the structural flexibility of the $A_2B_2O_7$ matrix. In $(Gd_{1-x}Nd_x)_2(Zr_{1-x}Ce_x)_2O_7$ series, the radius variation at B-site (Δr_B) is bigger than that of A-site (Δr_A) after Nd/Ce co-doping with equal quantity. In detail, since the radii of Nd^{3+} (VIII, 1.109 Å) and Ce^{4+} (VI, 0.87 Å) are larger than that of Gd^{3+} (VIII, 1.053 Å) and Zr^{4+} (VI, 0.72 Å), respectively, the Δr_B value ($\Delta r_B = 0.15$) is bigger than that of Δr_A ($\Delta r_A = 0.056$). It means that the average $r(A^{3+})/r(B^{4+})$ value of $(Gd_{1-x}Nd_x)_2(Zr_{1-x}Ce_x)_2O_7$ cannot exceed 1.4625. Therefore, the equal quantity Nd/Ce co-doped $Gd_2Zr_2O_7$ always presents disordered defect-fluorite structure in our previous work [24]. It was reported that the order-disorder structure can be substantially tailored by Sm/Ce co-doping with unequal quantity in $Gd_2Zr_2O_7$ according to the theory of average $r(A^{3+})/r(B^{4+})$ value [25]. However, the effects of the two structures on the chemical stability of co-doped ceramics have been seldom reported. It is essential to investigate the chemical stability difference of order-disorder structure, which can provide the guidance for preparing pyrochlore ceramics and then hopefully contribute to the HLWs safe immobilization.

In this work, Nd^{3+} and Ce^{4+} were employed to simulate trivalent actinides and tetravalent actinides respectively. Various unequal quantities of Nd/Ce co-doped $(Gd, Nd)_2(Zr, Ce)_2O_7$ ceramic series were prepared by wet chemistry route followed by heating treatment. It was systematically investigated the order-disorder phase transition, microstructure, and element composition of $(Gd, Nd)_2(Zr, Ce)_2O_7$ pyrochlore ceramics. Importantly, the chemical stability differences of typical order-disorder structure samples were evaluated by the static leaching test. The effect mechanism of order-disorder structure on the chemical stability was analyzed as well.

2. Experimental

2.1. Preparation of $(Gd, Nd)_2(Zr, Ce)_2O_7$ powders and ceramics

The Nd/Ce co-doped $(Gd, Nd)_2(Zr, Ce)_2O_7$ ceramics were designed as $(Gd_{1-x}Nd_x)_2(Zr_{1-y}Ce_y)_2O_7$ ($x + y = 1$), in which the x value grew in the range of 0–1 while y decreased from 1 to 0. Table 1 shows the serial number, nominal composition, and other details of $(Gd, Nd)_2(Zr, Ce)_2O_7$ series. The raw materials were commercially available $Gd(NO_3)_3\cdot 6H_2O$, $Nd(NO_3)_3\cdot 6H_2O$, $Zr(NO_3)_4\cdot 5H_2O$ and $Ce(NO_3)_3\cdot 6H_2O$ (all metal nitrates were purchased from Shanghai Aladdin Bio-Chem Technology Co., LTD, purity ≥99%). The raw materials were weighed according to the stoichiometric ratio of the chemical formula. After evenly mixing with alcohol by a planetary mill, the slurries were dried and calcined at 1000 °C for 10 h to synthesize $(Gd, Nd)_2(Zr, Ce)_2O_7$ powders. After that, the powders were shaped into tablets with about 3 mm thickness and 12 mm diameter. Lastly, the tablets were further compacted by cold isostatic pressing and subsequently sintered at 1500 °C for 24 h.

Table 1
Sample composition and preparation details for $(Gd_{1-x}Nd_x)_2(Zr_{1-y}Ce_y)_2O_7$ pyrochlore series.

Sample No.	Nominal composition	$x + y = 1$		Temperature (°C)	
		x	y	Powders	bulks
F1	$Gd_2Ce_2O_7$	0	1	1000	1500
F2	$(Gd_{0.9}Nd_{0.1})_2(Zr_{0.1}Ce_{0.9})_2O_7$	0.1	0.9	1000	1500
F3	$(Gd_{0.7}Nd_{0.3})_2(Zr_{0.3}Ce_{0.7})_2O_7$	0.3	0.7	1000	1500
F4	$(Gd_{0.5}Nd_{0.5})_2(Zr_{0.5}Ce_{0.5})_2O_7$	0.5	0.5	1000	1500
F5	$(Gd_{0.3}Nd_{0.7})_2(Zr_{0.7}Ce_{0.3})_2O_7$	0.7	0.3	1000	1500
P6	$(Gd_{0.1}Nd_{0.9})_2(Zr_{0.9}Ce_{0.1})_2O_7$	0.9	0.1	1000	1500
P7	$Nd_2Zr_2O_7$	1	0	1000	1500

2.2. Characterization

The phase structure of $(Gd, Nd)_2(Zr, Ce)_2O_7$ powders and ceramic bulks were tested by an X-ray diffractometer (XRD, X'Pert PRO, Netherlands) using Cu Kα radiation. The volume and cell parameters of the ceramics were quantified with the external standard method by analyzing the XRD results. A Raman spectrometer (InVia, Renishaw PLC, UK) was employed to obtain Raman spectra of ceramics. The microtopography and elemental distribution of ceramic bulks were observed by scanning electron microscopy attached with an energy dispersive spectrometer (SEM-EDS, TM-4000, Hitachi Inc.).

2.3. Chemical stability

The chemical stability of typical order-disorder ceramic samples (F5, P6) was evaluated by the standard Materials Characterization Center (MCC-1) method [27]. The MCC-1 ceramic samples were formed as a cylinder with a height of about 12 mm and a diameter of about 11 mm, suspended in the center of polytetrafluoroethylene (PTFE) liner of the hydrothermal reactor. And then, the cylindrical samples were immersed in deionized water at 90 °C for 1–42 days. The accumulative leaching time of solutions was 1, 3, 7, 14, 21, 28, 35 and 42 days, respectively. At the various leaching period, the leaching concentrations (Ci) of four elements (Gd, Nd, Zr, and Ce) in the leachates were measured by an inductively coupled plasma mass spectrometry (ICP-MS, Agilent 7700 ×, USA). The normalized elemental leaching rates LR_i ($g\cdot m^{-2}\cdot d^{-1}$) were calculated by the following Eq. (1):

$$LR_i = \frac{C_i \cdot V_l}{f_i \cdot \Delta t \cdot S} \tag{1}$$

where C_i (mg/L) is the leaching concentrations of element i, V_l (L) is the volume of deionized water, f_i (wt.%) means the mass percent of element i, Δt (day) is the cumulative leaching time, and S (m^2) signifies the surface area of the sample.

3. Results and discussion

3.1. XRD analysis of order-disorder structure

As the order-disorder structure of $A_2B_2O_7$ pyrochlore depends on the average $r(A^{3+})/r(B^{4+})$ value, the $r(A^{3+})/r(B^{4+})$ values of $(Gd_{1-x}Nd_x)_2(Zr_{1-y}Ce_y)_2O_7$ series were calculated as follow Eq. (2):

$$\frac{r\left(A^{3+}\right)}{r\left(B^{4+}\right)} = \frac{(1-x)r\left(Gd^{3+}\right) + xr\left(Nd^{3+}\right)}{(1-y)r\left(Zr^{4+}\right) + yr\left(Ce^{4+}\right)} \tag{2}$$

According to Eq. (2) and the $r(A^{3+})/r(B^{4+})$ value scope of order-disorder structure, the $r(A^{3+})/r(B^{4+})$ value and theoretical ordered or disordered structure type of $(Gd, Nd)_2(Zr, Ce)_2O_7$ series could be obtained, which were listed in Table 2. In $(Gd_{1-x}Nd_x)_2(Zr_{1-y}Ce_y)_2O_7$ ($x + y = 1$) system, the x value increased in the range of 0–1 while y value decreased from 1 to 0, then, the r_A value raised but the r_B value reduced. Namely, the $r(A^{3+})/r(B^{4+})$ value of the designed compositions gradually increased with Nd/Ce co-doping of unequal quantity, and the sample compositions exactly changed from

Table 2
The average r(A^{3+})/r(B^{4+}) radius ratio, cell parameters, volume, and phase structure of (Gd, Nd)$_2$(Zr, Ce)$_2$O$_7$ ceramics based on XRD patterns.

Sample No.	Nominal composition	Average r(A^{3+})/r(B^{4+})	Cell parameters(Å)	Volume (Å^3)	Phase structure
F1	$Gd_2Ce_2O_7$	1.2103	5.4275	159.78	Fluorite
F2	$(Gd_{0.9}Nd_{0.1})_2(Zr_{0.1}Ce_{0.9})_2O_7$	1.2381	5.4202	159.24	Fluorite
F3	$(Gd_{0.7}Nd_{0.3})_2(Zr_{0.3}Ce_{0.7})_2O_7$	1.2967	5.3991	157.39	Fluorite
F4	$(Gd_{0.5}Nd_{0.5})_2(Zr_{0.5}Ce_{0.5})_2O_7$	1.3597	5.3845	156.11	Fluorite
F5	$(Gd_{0.3}Nd_{0.7})_2(Zr_{0.7}Ce_{0.3})_2O_7$	1.4277	5.3746	155.25	Fluorite
P6	$(Gd_{0.1}Nd_{0.9})_2(Zr_{0.9}Ce_{0.1})_2O_7$	1.5012	10.6782	1217.56	Pyrochlore
P7	$Nd_2Zr_2O_7$	1.5403	10.6566	1210.19	Pyrochlore

$Gd_2Ce_2O_7$ (F1 sample) to $Nd_2Zr_2O_7$ (P7 sample). Corresponding to the seven compositions, the theoretical structure transformed from the disordered defect-fluorite structure (F1–F5) to the ordered pyrochlore structure (P6, P7) when the average r(A^{3+})/r(B^{4+}) value exceeded 1.4625.

As shown in Fig. 1, all sample powders synthesized at 1000 °C present all characteristic peaks of the typical defect-fluorite phase. It indicates that the Nd/Ce co-doping (Gd, Nd)$_2$(Zr, Ce)$_2$O$_7$ series have been successfully synthesized by wet chemistry route followed by heating treatment. Fig. 2 displays XRD patterns of (Gd, Nd)$_2$(Zr, Ce)$_2$O$_7$ ceramic bulks sintered at 1500 °C for 24 h. Compared with the XRD patterns of powders, P6 and P7 compositions ($Gd_{0.2}Nd_{0.8}Zr_{0.8}Ce_{0.2}$ and $Nd_2Zr_2O_7$) show the ordered pyrochlore structure which can be identified by the typical super-lattice peaks of (111), (311), (331), (511) and (531) planes [5,28]. Considering that these peaks always exist in ordered pyrochlore structure, therefore, the absence of the five super-lattice peaks indicates the disordered defect-fluorite structure of F1–F5 ceramic samples sintered at 1500 °C for 24 h. It is observed that the XRD results of ceramic bulks are accurately consistent with the theoretical conclusion of the order-disorder phase structure type listed in Table 2. Besides, from F1 to P7 samples, the diffraction peaks slightly shift to the right, which can be seen in the right enlarged view of Fig. 2. In specific, based on the radii of Gd^{3+} (VIII, 1.053 Å), Nd^{3+} (VIII, 1.109 Å), Zr^{4+} (VI, 0.72 Å) and Ce^{4+} (VI, 0.87 Å), it is calculated that the radii increment value of A-site ($\Delta r_A = +0.056$) is smaller than the radii decrement value of B-site ($\Delta r_B = -0.15$) as sample gradually changed from $Gd_2Ce_2O_7$ (F1 samples) to $Nd_2Zr_2O_7$ (P7 samples). That is to say, the average anion radius becomes smaller with unequal quantities of Nd/Ce co-doping to $Gd_2Zr_2O_7$ matrix, and then, leads to the decrease of the inter-planar spacing in the crystal structure. Resultantly, the diffraction peaks shift toward a higher 2θ angle according to the Bragg equation. It could be naturally deduced that the unequal quantity of Nd and Ce have been incorporated into the Gd- and Zr-sites of $Gd_2Zr_2O_7$, respectively.

Based on the XRD results of ceramic bulks, the cell parameters and volumes of (Gd, Nd)$_2$(Zr, Ce)$_2$O$_7$ ceramics are obtained and listed in Table 2. It is well known that the cell parameters and volumes are closely relevant to the phase structure type. Apparently, the cell parameters of the pyrochlore phase are nearly twice as big as that of the defect-fluorite phase, which stays in step with the theory of order-disorder structure. The cell parameters and volume decrease with the increase of average r(A^{3+})/r(B^{4+}) value for F1–F5 samples. Due to the unequal quantity co-doped of Ne/Ce in the ceramics, the radius variation of Δr_A is less than that of Δr_B,

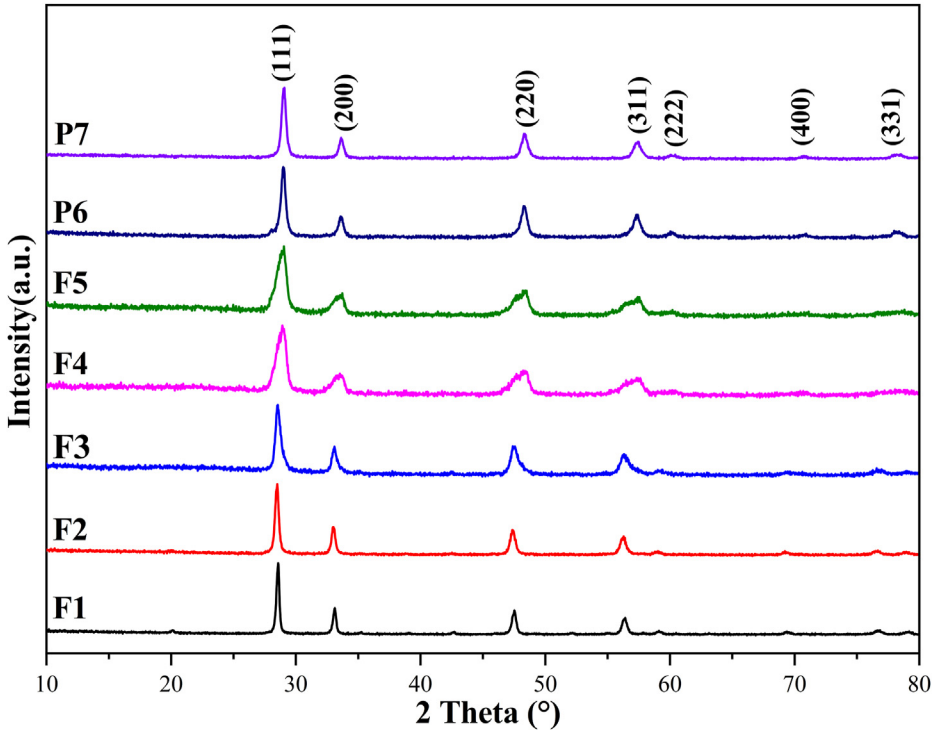

Fig. 1. XRD patterns of (Gd, Nd)$_2$(Zr, Ce)$_2$O$_7$ powders synthesized at 1000 °C for 10 h.

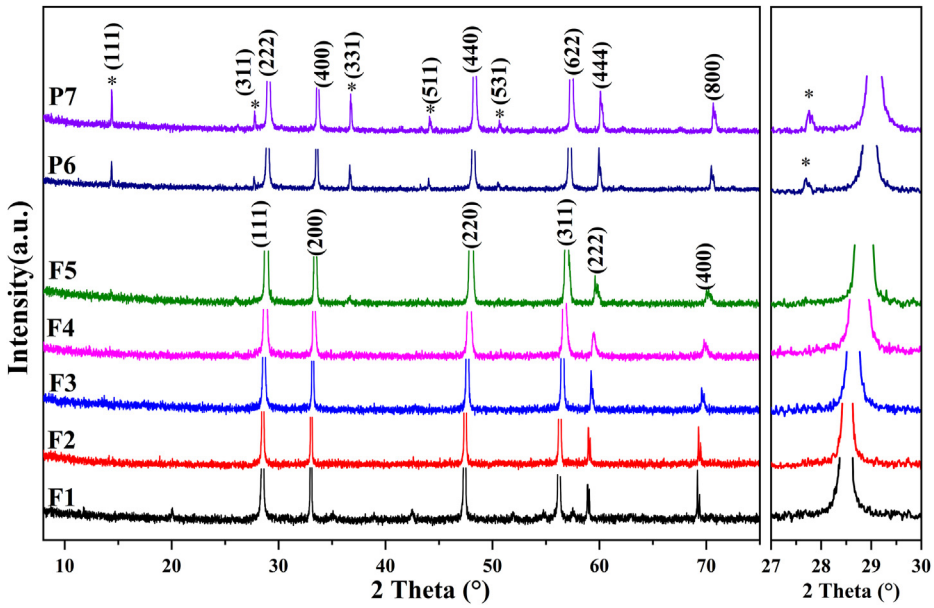

Fig. 2. XRD patterns of (Gd, Nd)$_2$(Zr, Ce)$_2$O$_7$ ceramic bulks sintered at 1500 °C for 24 h; the asterisks (*) mark the super-lattice peaks of the pyrochlore phase.

and then the cell parameters apparently decrease. It can further account for the right shift of the diffraction peaks for F1–P7 samples.

3.2. Raman spectroscopy analysis

Fig. 3 shows Raman spectra of (Gd, Nd)$_2$(Zr, Ce)$_2$O$_7$ ceramic bulks sintered at 1500 °C for 24 h. It was previously reported that the $A_2B_2O_7$ pyrochlore structure possesses six Raman vibration modes, namely A_{1g}, E_g, and four F_{2g} modes [28,29]. In this work, the Raman vibration peaks at ~300 cm^{-1} and ~520 cm^{-1} belong to E_g and A_{1g} modes, respectively. And the F_{2g} vibration peaks appear at ~374 cm^{-1}, ~400 cm^{-1}, ~480-500 cm^{-1} and ~580-600 cm^{-1} [30–32]. In particular, a broad peak observed in the Raman spectrum of P7 sample can be resolved into two components at ~500 and ~520 cm^{-1}, which are assigned as F_{2g} and A_{1g} modes, respectively [31]. Table 3 lists the corresponding vibration types of various modes. As shown in Fig. 3, the ordered pyrochlore structure of P6 and P7 samples differs in Raman vibration modes from the disordered defect-fluorite structure of F1–F5 samples. It was reported

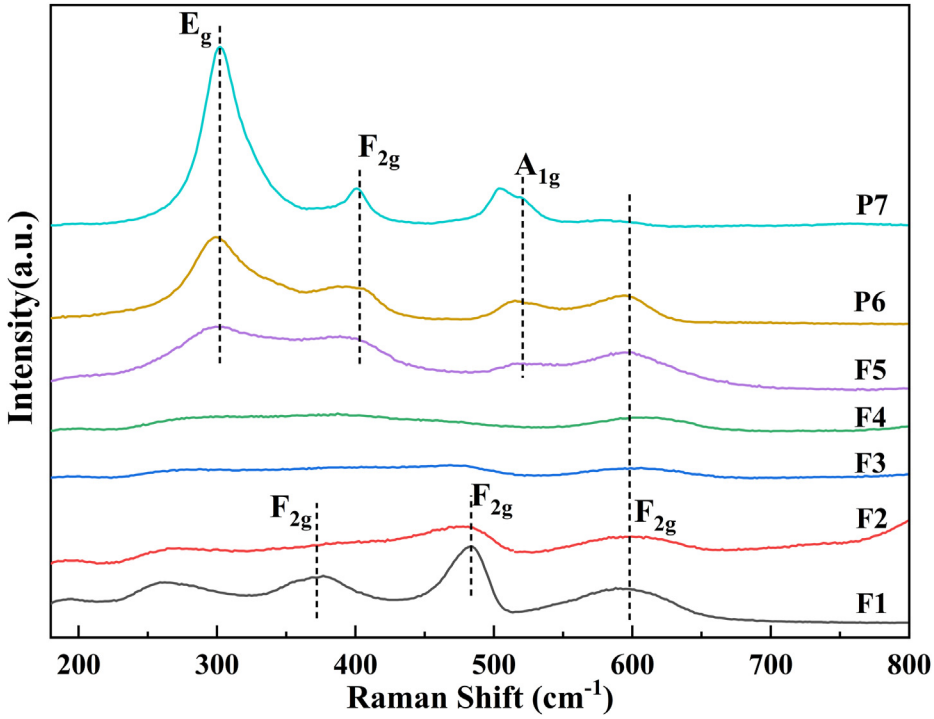

Fig. 3. Raman spectra of (Gd, Nd)$_2$(Zr, Ce)$_2$O$_7$ ceramic bulks sintered at 1500 °C for 24 h.

Table 3
Raman mode frequencies with symmetry character and vibration types.

Frequency (cm^{-1})	Symmetry	Vibration type
~301	E_g	O-(Zr, Ce)–O bending
~362	F_{2g}	O-(Gd, Nd)-O bending
~400	F_{2g}	O-(Zr, Ce)–O stretching
~500	F_{2g}	O-(Zr, Ce)–O bending
~521	A_{1g}	Mostly O-(Zr, Ce)–O bending with mixture of O-(Zr, Ce)–O and O-(Gd, Nd)-O stretching
~602	F_{2g}	O-(Zr, Ce)–O bending

that the intensity of E_g and A_{1g} modes usually depended on the order degree of the $A_2B_2O_7$ structure [31,33]. Because the phase structure type of the as-prepared samples transforms from the disordered defect-fluorite phase to the ordered pyrochlore phase with increasing the average $r(A^{3+})/r(B^{4+})$ value, E_g and A_{1g} vibration peaks become more and more strong and sharp. It is attributed to the decrease of cationic anti-site disorder degree resulting in the order of oxygen occupation, which narrows the Raman vibration modes [28,31]. In addition, for F5, P6 and P7 samples, the F_{2g} mode at ~400 cm^{-1} displays the same variation trend as E_g and A_{1g} modes, which is ascribed to the O-(Zr, Ce)–O stretching vibration.

Besides, the vibration peaks of F1 sample ($Gd_2Ce_2O_7$) present higher intensity than other compositions with disordered structure (F2–F5), especially two distinct F_{2g} modes at 374 and 484 cm^{-1}, which are mostly assigned to O-Gd-O bending and O–Ce–O bending, respectively. It seems to contradict with the Raman vibration factor group prediction that the defect fluorites have only a single broad band [28,33]. However, any defect fluorite has minor pyrochlore domains due to kinetic limitation factors and thermal history of reactants [34]. Therefore, pyrochlore phase as a superstructure of fluorite phase may exist as microdomains within F1–F5 defect-fluorite samples in this situation. That is the reason XRD classifies F1–F5 samples as disordered fluorite phase and Raman spectra studies reveal the existence of ordering variation modes for these compositions. In addition, the Raman vibration modes shift to a higher wavenumber with the increase of the $r(A^{3+})/r(B^{4+})$ value from F1 to P7 samples. Notably, the third F_{2g} mode moves from ~485 cm^{-1} to ~500 cm^{-1}. It could be explained by Nd/Ce co-doping in the crystal lattice of the $Gd_2Zr_2O_7$ matrix. With the increase of average $r(A^{3+})/r(B^{4+})$ value from F1 to P7 composition, the cell parameters decrease accordingly and then the Raman wave vector distinctly increases. Raman analysis results further confirmed that unequal quantity Ne/Ce co-doping can tailor the order-disorder structure, meanwhile, Nd/Ce can simultaneously replace the Gd-/Zr-sites of the $Gd_2Zr_2O_7$ crystal structure, respectively.

3.3. SEM-EDS analysis

To examine the compactness behavior and microstructure of the sample, the fractography of $(Gd, Nd)_2(Zr, Ce)_2O_7$ ceramic series was observed after sintering at 1500 °C for 24 h, as shown in Fig. 4. It is displayed that the grain size of the ordered structure for P6 and P7 samples seems larger than that of the disordered structure for F1–F5 samples. Besides, all samples show the characteristic of porous microtopography, in which the pore size also tends to decrease with increasing average $r(A^{3+})/r(B^{4+})$ value (F1 to P7). However, all ceramic samples present single-phase and transgranular fractures.

The typical samples with disordered and ordered structure (F5 and P6) were analyzed to elucidate the element composition and distribution by EDS detection. Four spots were selected on the representative fracture surface SEM image to calculate the average atomic ratio. The chosen spots are signed in Fig. 5(a)-(b), and the calculated atomic ratio results are tabular below the figure. The table shows that the atomic ratios of Gd/Ce and Nd/Zr for both samples nearly attain the same value. And the element contents measured by EDS basically accord with the nominal chemical composition of the samples. Besides, the mapping distributions of four elements (Gd, Nd, Zr, Ce) for the two samples are shown in Fig. 5(c)–(j). Clearly, the four elements are evenly distributed in the selected region except for some pits and holes. It is universally acknowledged that electronic energy is hard to reach these micropores and flaws during EDS examination. SEM-EDS analysis reconfirmed that Nd and Ce can be co-incorporated into the lattice of the $Gd_2Zr_2O_7$ matrix with unequal quantity co-doping.

3.4. Chemical stability

It is exceedingly beyond dispute that pyrochlore ceramics as nuclear waste forms need excellent chemical stability to prevent radionuclides leakage under geological repository environment [35–38]. The widely recognized MCC-1 leaching test was employed to investigate the chemical stability difference of F5 sample with disordered structure and of P6 sample with ordered structure. Fig. 6 shows the LR_i line chart of four elements (Gd, Nd, Zr, and Ce) in the F5 and P6 ceramic bulks leached at 90 °C under deionized water. The LR_i values of the four elements all appear a decreasing tendency before 14 days duration. With the prolongation of leaching period, the leaching rates drop gently and converge to constant values. By comparison with LR_i (i = Nd, Zr, and Ce), the LR_{Gd} value is the highest, about 10^{-3} g m^{-2} d^{-1} at 1-day period (seen in Fig. 6(a)). As illustrated in Fig. 6(b), the LR_{Nd} value after 1-day is 10^{-4} g m^{-2} d^{-1}, while it drops to 10^{-6} at a 7-day duration. Also, the LR_{Ce} value almost stays the same trend as the LR_{Nd} value, while LR_{Ce} is below one order of magnitude than LR_{Nd} for 1–7 days durations, as shown in Fig. 6(d). LR_{Zr} of the F5 sample converges to about 10^{-7} order magnitude at the 14-day duration, which is the smallest among the four elements (seen in Fig. 6(c)), and the Zr^{4+}concentration of the leachate cannot be detected even after 14 days duration. Similarly, the Zr^{4+}concentration cannot be detected at any leaching period for the ordered P6 sample. A weaker bond of Gd–O and stronger Zr–O bond in $Gd_2Zr_2O_7$ matrix can directly contribute to their highest and lowest elemental leaching rate [39], respectively. The high LR_i value in the early leaching time is theoretically attributed to the grain boundary dissolution of ceramics [39,40], which indirectly suggests that the crystal cell or grain itself is pretty stable. After 1–7 days periods of soaking, with the precipitation and dissolution of the maskant [41], all elements in the pyrochlore crystal cell remain relatively stable without apparent dissolution and diffusion.

Table 4 lists the 7-day LR_i magnitudes of similar pyrochlore ceramic nuclear waste forms in the literatures and this work. The LR_{Gd}, LR_{Nd} and LR_{Ce} values of the disordered structure are almost lower than that of the ordered structure by one order of magnitude in this work. The phenomenon is generally in agreement with the results reported in the literatures, in which the LR_{Gd} and LR_{Zr} values in disordered structure fall in 10^{-5} and 10^{-6}-10^{-7} g m^{-2} d^{-1} while change within the 10^{-3}-10^{-4} and 10^{-4}-10^{-6} scope in ordered

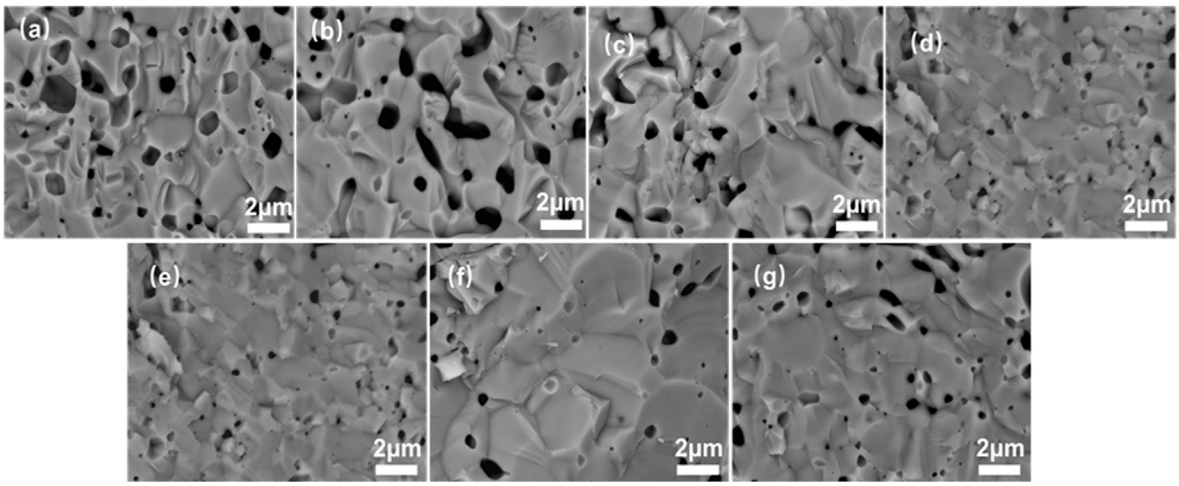

Fig. 4. Fracture surface SEM images of $(Gd, Nd)_2(Zr, Ce)_2O_7$ ceramic bulks sintered at 1500 °C for 24 h: (a) F1, (b) F2, (c) F3, (d) F4, (e) F5, (f) P6, (g) P7.

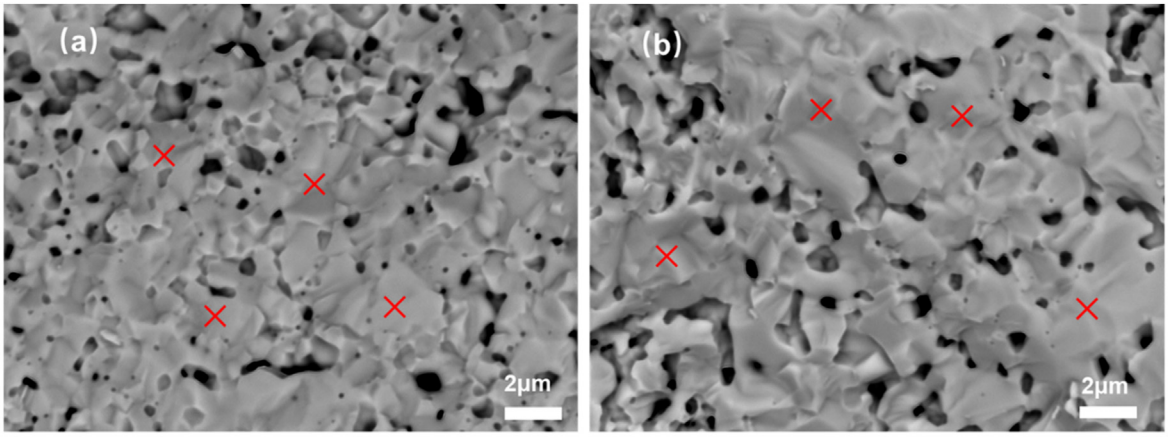

Elements	Gd	Nd	Zr	Ce
F5-Atomic(%)	6.86	15.48	16.47	7.01
P6-Atomic(%)	2.44	18.52	19.86	2.49

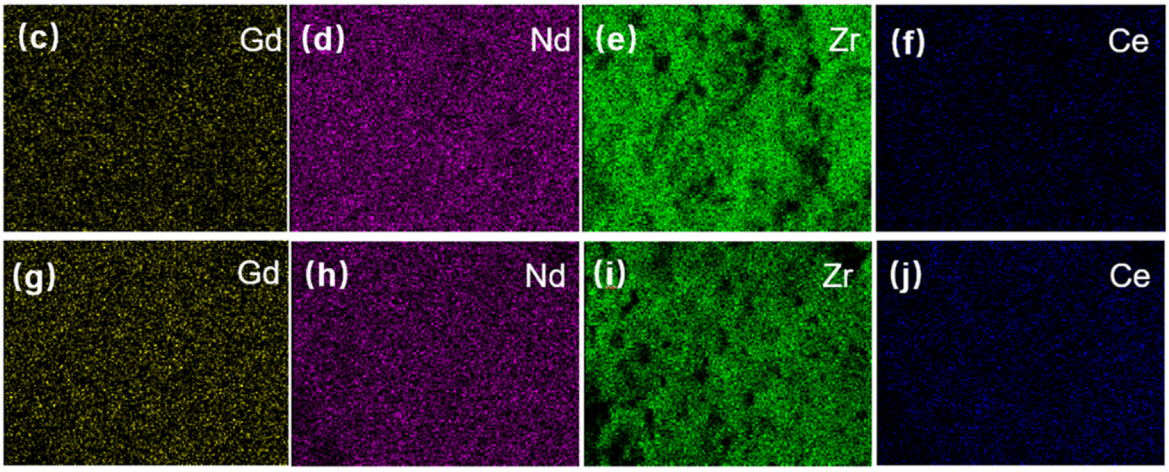

Fig. 5. SEM-EDS images of F5 (disordered, $(Gd_{0.3}Nd_{0.7})_2(Zr_{0.7}Ce_{0.3})_2O_7$) and P6 (ordered, $(Gd_{0.1}Nd_{0.9})_2(Zr_{0.9}Ce_{0.1})_2O_7$) ceramic bulks sintered at 1500 °C for 24 h, (a)–(b): representative SEM images and EDS spotting sites of F5 and P6 samples, (c)–(f) and (g)–(j): elemental mapping images of Gd, Nd, Zr, Ce for F5 and P6, respectively.

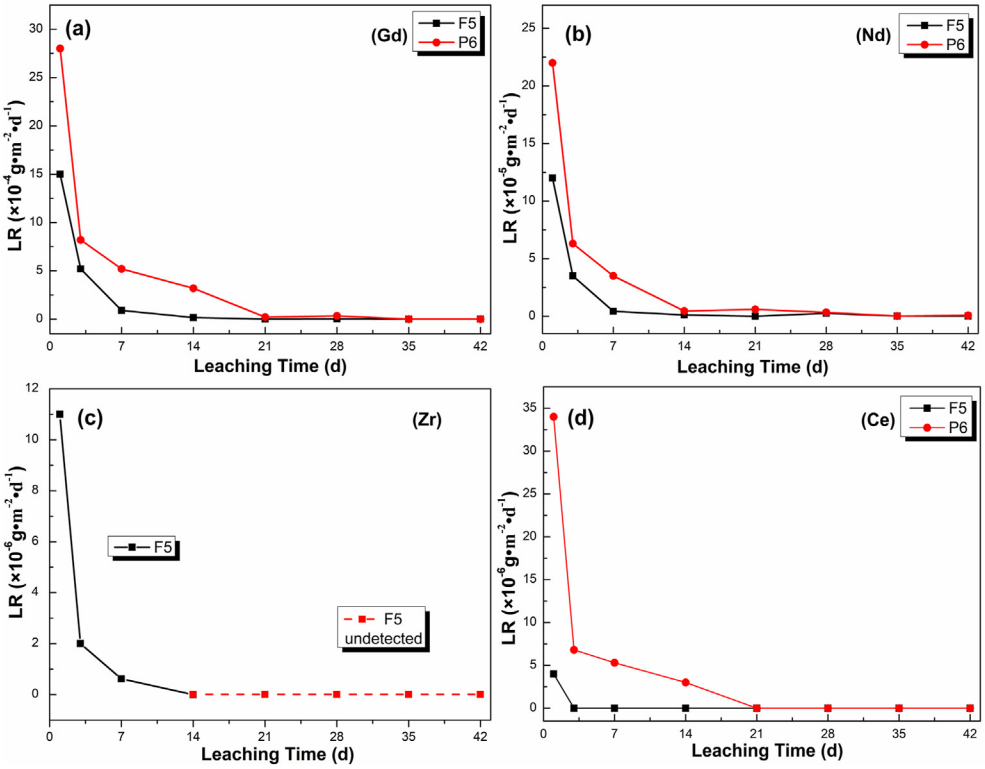

Fig. 6. Normalized elemental leaching rates of F5 (disordered, $(Gd_{0.3}Nd_{0.7})_2(Zr_{0.7}Ce_{0.3})_2O_7$) and P6 (ordered, $(Gd_{0.1}Nd_{0.9})_2(Zr_{0.9}Ce_{0.1})_2O_7$) ceramic bulks: (a) Gd, (b) Nd, (c) Zr and (d) Ce.

Table 4
The 7-day LR_i values of order-disorder structure from the literatures.

Structure type	Leaching test	Sample Composition	Normalized release rates ($g \cdot m^{-2} \cdot d^{-1}$)				Reference
			Gd	Nd	Zr	Ce	
Disorder	90 °C, deionized water	$(Gd_{0.3}Nd_{0.7})_2(Zr_{0.7}Ce_{0.3})_2O_7$	10^{-5}	10^{-6}	10^{-7}	10^{-7}	This paper
Order	90 °C, deionized water	$(Gd_{0.1}Nd_{0.9})_2(Zr_{0.9}Ce_{0.1})_2O_7$	10^{-4}	10^{-5}	–	10^{-6}	This paper
Disorder	90 °C, deionized water	$(Gd_{0.5}Nd_{0.5})_2(Zr_{0.5}Ce_{0.5})_2O_7$	10^{-5}	10^{-5}	10^{-7}	–	[24]
Disorder	90 °C, deionized water	$(Gd_{0.25}Sm_{0.75})_2(Zr_{0.75}Ce_{0.25})_2O_7$	10^{-5}	–	10^{-6}	10^{-6}	[25]
Order	70 °C, deionized water	$Gd_2Zr_2O_7$	10^{-4}	–	10^{-5}	–	[39]
Order	90 °C, deionized water	$Gd_2Zr_2O_7$	10^{-3}-10^{-4}	–	10^{-4}-10^{-6}	–	[42]

structure, respectively. Hence, it is suggested that the chemical stability of disordered defect-fluorite structure is superior to that of ordered pyrochlore structure. Such chemical stability difference may be explained by the force constant and the structural transition. In this work, with increasing the $r(A^{3+})$ value and decreasing the $r(B^{4+})$ value from the disordered structure (F5) to the ordered structure (P6), the force constants of (Gd, Nd)-O and (Zr, Ce)—O that depend on the spatial ordering of the coordination polyhedron may vary with the bond characteristics and their chemical environment [24,43]. Besides, for the disorder-order phase transition of the two samples, the oxygens/vacancies mixed at 8c Wyckoff site for the disordered structure were changed to the oxygen anions at 8b/48f equivalent sites and vacancies at 8a site when transformed to the ordered structure. And the mixing occupation by A/B cations at 4a equivalent positions for the disordered structure will be reassigned and coordinated with oxygens/vacancies to form 16c and 16d sites in the ordered structure [5,44,45]. Resultantly, the vacancies, oxygens and cations in the disordered defect-fluorite structure become closer, even the packing degree of cations and oxygen anions get higher than that of the ordered pyrochlore structure, and the force constant gets stronger gradually. Meanwhile, the disordered defect-fluorite structure could not provide an ion channel for leaching elements due to the lack of oxygen vacancy, resulting in the excellent chemical stability of the disordered structure.

4. Conclusions

The $(Gd_{1-x}Nd_x)_2(Zr_{1-y}Ce_y)_2O_7$ $(x + y = 1)$ ceramic nuclear waste forms with Nd/Ce unequal quantity co-doping were designed and successfully prepared to tailor the order-disorder structure. As the average $r(A^{3+})/r(B^{4+})$ value increased, the structure type of ceramics was transformed from the disordered defect-fluorite phase to the ordered pyrochlore phase. It was concluded that Nd^{3+} and Ce^{4+} could be co-incorporated into Gd- and Zr-sites of $Gd_2Zr_2O_7$ matrix, and the ordered or disordered structure was entirely tailored by the unequal quantity of Nd/Ce co-doping. All the elements in the samples with ordered or disordered structure were almost uniformly distributed. And the atomic ratios of the different structures remarkably accorded with the theoretical chemical composition. The leaching results implied that $(Gd, Nd)_2(Zr, Ce)_2O_7$ pyrochlore ceramics had excellent chemical stability. The LR_i value of the four elements was gradually stabilized with a relatively low

constant of about 10^{-5}–10^{-7} g·m^{-2}·d^{-1} after a 7-day duration. In particular, the LR_i value of the disordered structure was lower about one order of magnitude than that of the ordered structure, indicating that the chemical stability of disordered defect-fluorite structure is superior to that of ordered pyrochlore structure. The chemical stability difference of the two structures may provide the guidance for preparing pyrochlore ceramic nuclear waste forms with good performances.

Declaration of competing interest

The authors declare that they have no known competing financial interests or personal relationships that could have appeared to influence the work reported in this paper.

Acknowledgements

We received a great deal of support and assistance from the National Natural Science Foundation of China (Nos. 12075195 and 11705153), the Foundation of Laboratory of National Defense Key Discipline for Nuclear Waste and Environmental Safety of Southwest University of Science and Technology (No. 17kfhk05).

References

[1] E. Sartori, Nuclear data for radioactive waste management, Ann. Nucl. Energy 62 (2013) 579–589.
[2] M.M. Abu-Khader, Recent advances in nuclear power: a review, Prog. Nucl. Energy 51 (2009) 225–235.
[3] A.E. Ringwood, S.E. Kesson, N.G. Ware, W.O. Hibberson, Immobilisation of high level nuclear reactor wastes in SYNROC, Nature 278 (1979) 219–223.
[4] E.R. Vance, G.R. Lumpkin, M.L. Carter, D.J. Cassidy, C.J. Ball, R.A. Day, B.D. Begg, Incorporation of uranium in zirconolite ($CaZrTi_2O_7$), J. Am. Ceram. Soc. 85 (2002) 1853–1859.
[5] R.C. Ewing, W.J. Weber, J. Lian, Nuclear waste disposal—pyrochlore ($A_2B_2O_7$): nuclear waste form for the immobilization of plutonium and "minor" actinides, J. Appl. Phys. 95 (2004) 5949–5971.
[6] N.U. Navi, S.V. Ushakov, R.Z. Shneck, M.H. Mintz, Yttrium substitution in $MTiO_3$ (M=Ca, Sr, Ba and Ca+Sr+Ba) perovskites and implication for incorporation of fission products into ceramic waste forms, J. Am. Ceram. Soc. 94 (2011) 3112–3116.
[7] G.J. Mccarthy, W.B. White, D.E. Pfoertsch, Synthesis of nuclear waste monazites, ideal actinide hosts for geologic disposal, M.R.S. Bull. 13 (1978) 1239–1245.
[8] R.C. Ewing, Nuclear waste forms for actinides, Proc. Natl. Acad. Sci. Unit. States Am. 96 (1999) 3432–3439.
[9] W.J. Weber, A. Navrotsky, S. Stefanovsky, E.R. Vance, E. Vernaz, Materials science of high-level nuclear waste immobilization, M.R.S. Bull. 34 (2009) 46–53.
[10] M. Jafar, S.B. Phapale, B.P. Mandal, R. Mishra, A.K. Tyagi, Preparation and structure of Uranium-incorporated $Gd_2Zr_2O_7$ compounds and their thermodynamic stabilities under oxidizing and reducing conditions, Inorga. Chem. 54 (2015) 9447–9457.
[11] M. Lang, F. Zhang, J. Zhang, J. Wang, J. Lian, W.J. Weber, B. Schuster, C. Trautmann, R. Neumann, R.C. Ewing, Review of $A_2B_2O_7$ pyrochlore response to irradiation and pressure, Nucl. Instrum. Methods Phys. Res. Sect. B Beam Interact. Mater. Atoms 268 (2010) 2951–2959.
[12] K.E. Sickafus, L. Minervini, R.W. Grimes, J.A. Valdez, M. Ishimaru, F. Li, K.J. Mcclellan, T. Hartmann, Radiation tolerance of complex oxides, Science 289 (2000) 748–751.
[13] S.X. Wang, L.M. Wang, R.C. Ewing, G.S. Was, G.R. Lumpkin, Ion irradiation-induced phase transformation of pyrochlore and zirconolite, Nucl. Instrum. Methods Phys. Res. Sect. B Beam Interact. Mater. Atoms 148 (1999) 704–709.
[14] F.W. Poulsen, M. Glerup, P. Holtappels, Structure, Raman spectra and defect chemistry modelling of conductive pyrochlore oxides, Solid State Ionics 135 (2000) 595–602.
[15] A. Garbout, S. Bouattour, A.W. Kolsi, Sol–gel synthesis, structure characterization and Raman spectroscopy of $Gd_{2-2x}Bi_{2x}Ti_2O_7$ solid solutions, J. Alloys Compd. 469 (2009) 229–236.
[16] R.C. Ewing, W.J. Weber, F.W. Clinard, Radiation effects in nuclear waste forms for high-level radioactive waste, Prog. Nucl. Energy 29 (1995) 63–127.
[17] W.J. Weber, R.C. Ewing, Plutonium immobilization and radiation effects, Science 289 (2000) 2051.
[18] X. Wang, K. Jiang, L. Zhou, Characterization, and phase stability of pyrochlore $(Nd_{1-x}Ce_x)_2Zr_2O_{7+y}$ (x = 0-1), J. Nucl. Mater. 458 (2015) 156–161.
[19] J. Lian, K.B. Helean, B.J. Kennedy, L.M. Wang, A. Navrotsky, R.C. Ewing, Effect of structure and thermodynamic stability on the response of lanthanide stannate pyrochlores to ion beam irradiation, J. Phys. Chem. B 110 (2006) 2343–2350.
[20] B.J. Wuensch, K.W. Eberman, C. Heremans, E.M. Ku, P. Onnerud, E.M.E. Yeo, S.M. Haile, J.K. Stalick, J.D. Jorgensen, Connection between oxygen-ion conductivity of pyrochlore fuel-cell materials and structural change with composition and temperature, Solid State Ionics 129 (2016) 111–133.
[21] Y.H. Zhang, M. Xie, F. Zhou, H. Zhang, X.K. Zhao, Phase structure and thermophysical properties of co-doped $La_2Zr_2O_7$ ceramics for thermal barrier coatings, Ceram. Int. 38 (2012) 3607–3612.
[22] B.P. Mandal, A.K. Tyagi, Preparation and high temperature-XRD studies on a pyrochlore series with the general composition $Gd_{2-x}Nd_xZr_2O_7$, J. Alloys Compd. 437 (2007) 260–263.
[23] S.J. Patwe, B.R. Ambekar, A.K. Tyagi, Synthesis, characterization and lattice thermal expansion of some compounds in the system $Gd_2Ce_xZr_{2-x}O_7$, J. Alloys Compd. 389 (2005) 243–246.
[24] J. Wang, J. Wang, Y. Zhang, Y. Li, Y. Teng, Z. Wang, H. Tan, Flux synthesis and chemical stability of Nd and Ce co-doped $(Gd_{1-x}Nd_x)_2(Zr_{1-x}Ce_x)_2O_7$ ($0 \le x \le 1$) pyrochlore ceramics for nuclear waste forms, Ceram. Int. 43 (2017) 17064–17070.
[25] J. Wang, J. Wang, Y. Zhang, Y. Wei, K. Zhang, H. Tan, X. Liang, Order-disorder phase structure, microstructure, and aqueous durability of $(Gd, Sm)_2(Zr, Ce)_2O_7$ ceramics for immobilizing actinides, Ceram. Int. 45 (2019) 17898–17904.
[26] M. Jafar, S.B. Phapale, S. Nigam, S.N. Achary, A.K. Tyagi, Implication of aliovalent cation substitution on structural and thermodynamic stability of $Gd_2Ti_2O_7$: Experimental and theoretical investigations, J. Alloys Compd. 859 (2020) 157781.
[27] ASTM C1220-98, Standard Test Method for Static Leaching of Monolithic Waste Forms for Disposal of Radioactive Waste, 1998. West Conshohocken, PA, USA.
[28] M. Jafar, S.B. Phapale, B.P. Mandal, M. Roy, A.K. Tyagi, Effect of temperature on phase evolution in $Gd_2Zr_2O_7$: a potential matrix for nuclear waste immobilization, J. Alloys Compd. 867 (2021) 159032.
[29] B.P. Mandal, N. Garg, S.M. Sharma, A.K. Tyagi, Solubility of ThO_2 in $Gd_2Zr_2O_7$ pyrochlore: XRD, SEM and Raman spectroscopic studies, J. Nucl. Mater. 392 (2009) 95–99.
[30] A.A. Yastrebtsev, V.V. Popov, A.P. Menushenkov, A.I. Beskrovnyi, D. Neov, Kirill Ponkratov, I.V. Shchetinin, Comparative neutron and X-ray diffraction analysis of anionic and cationic ordering in rare-earth zirconates (Ln= La, Nd, Tb, Yb, Y), J. Alloy. Comp 832 (2020) 154863.
[31] B.P. Mandal, A. Banerji, V. Sathe, S.K. Deb, A.K. Tyagi, Order-disorder transition in $Nd_{2-y}Gd_yZr_2O_7$ pyrochlore solid solution: an X-ray diffraction and Raman spectroscopic study, J. Solid State Chem. 180 (2007) 2643–2648.
[32] X. Shu, L. Fan, X. Lu, Y. Xie, Y. Ding, Structure and performance evolution of the system $(Gd_{1-x}Nd_x)_2(Zr_{1-y}Ce_y)_2O_7$ ($0 \le x$, $y \le 1.0$), J. Eur. Ceram. Soc. 35 (2015) 3095–3102.
[33] L. Kong, I. Karatchevtseva, D.J. Gregg, M.G. Blackford, R. Holmes, G. Triani, $Gd_2Zr_2O_7$ and $Nd_2Zr_2O_7$ pyrochlore prepared by aqueous chemical synthesis, J. Eur. Ceram. Soc. 33 (2013) 3273–3285.
[34] C. Nandi, A.K. Poswal, M. Jafar, S. Kesari, P.G. Behere, Effect of Ce^{4+}-substitution at A and B sites of $Nd_2Zr_2O_7$: a study for plutonium incorporation in pyrochlores, J. Nucl. Mater. 539 (2020) 152342.
[35] K.L. Smith, G.R. Lumpkin, M.G. Blackford, R.A. Day, K.P. Hart, The durability of synroc, J. Nucl. Mater. 190 (1992) 287–294.
[36] Y. Zhang, M.W.A. Stewart, H. Li, M.L. Carter, E.R. Vance, S. Moricca, Zirconolite-rich titanate ceramics for immobilization of actinides-waste form/H.I.P. can interactions and chemical durability, J. Nucl. Mater. 395 (2009) 69–74.
[37] C. Poinssot, S. Gin, Long-term Behavior Science: the cornerstone approach for reliably assessing the long-term performance of nuclear waste, J. Nucl. Mater. 420 (2012) 182–192.
[38] D. Horlait, L. Claparede, F. Tocino, N. Clavier, J. Ravaux, S. Szenknect, R. Podor, N. Dacheux, Environmental SEM monitoring of $Ce_{1-x}Ln_xO_{2-x/2}$ mixed-oxide microstructural evolution during dissolution, J. Mater. Chem. A. 2 (2014) 5193–5203.
[39] X. Lu, L. Fan, X. Shu, S. Su, D. Yi, F. Yi, Phase evolution and chemical durability of co-doped $Gd_2Zr_2O_7$ ceramics for nuclear waste forms, Ceram. Int. 41 (2015) 6344–6349.
[40] D. Caurant, O. Majérus, P. Loiseau, I. Bardez, N. Baffier, J.L. Dussossoy, Long-term Behavior Science: the cornerstone approach for reliably assessing the long-term performance of nuclear waste, J. Nucl. Mater. 354 (2006) 143–162.
[41] S. Gin, P. Jollivet, M. Fournier, F. Angeli, P. Frugier, T. Charpentier, Origin and consequences of silicate glass passivation by surface layers, Nat. Commun. 6 (2015) 6360.
[42] K. Liu, K. Zhang, T. Deng, W. Li, B. Luo, H. Zhang, Preparation of $Gd_2Zr_2O_7$ nanoceramics from two-step thermal treatment and the aqueous durability analysis, Ceram. Int. 46 (2020) 13040–13046.
[43] M.T. Vandenborre, E. Husson, J.P. Chatry, D. Michel, Rare-earth titanates and stannates of pyrochlore structure: vibrational spectra and force fields, J. Raman Spectrosc. 14 (1983) 63–71.
[44] D.J. Gregg, Y. Zhang, Z. Zhang, I. Karatchevtseva, G. Triani, M.G. Blackford, G. Triani, G.R. Lumpkin, E.R. Vance, Crystal chemistry and structures of uranium-doped gadolinium zirconates, J. Nucl. Mater. 438 (2013) 144–153.
[45] Y.H. Lee, H.S. Sheu, J.P. Deng, H.-C.I. Kao, Preparation and fluorite-pyrochlore phase transformation in $Gd_2Zr_2O_7$, J. Alloys Compd. 487 (2009) 595–598.